

Key Points:

- Estimating the bathymetry significantly improves the accuracy of tides in a global model
- The computational effort of parameter estimation is reduced by replacing the model grid with a coarser grid
- Further reduction in the computational effort of the parameter estimation is obtained by reducing the number of parameters to be estimated

Correspondence to:

X. Wang,
X.Wang-13@tudelft.nl

Citation:

Wang, X., Verlaan, M., Apecechea, M. I., & Lin, H. X. (2021). Computation-efficient parameter estimation for a high-resolution global tide and surge model. *Journal of Geophysical Research: Oceans*, 126, e2020JC016917. <https://doi.org/10.1029/2020JC016917>

Received 26 OCT 2020

Accepted 23 FEB 2021

Computation-Efficient Parameter Estimation for a High-Resolution Global Tide and Surge Model

Xiaohui Wang¹ , Martin Verlaan^{1,2} , Maialen Irazoqui Apecechea², and Hai Xiang Lin¹ 

¹Delft Institute of Applied Mathematics, Delft University of Technology, Delft, The Netherlands, ²Deltares, Delft, The Netherlands

Abstract In this study, a computation-efficient parameter estimation scheme for high-resolution global tide models is developed. The method is applied to Global Tide and Surge Model with an unstructured grid with a resolution of about 2.5 km in the coastal area and about 4.9 million cells. The estimation algorithm uses an iterative least squares method, known as DUD. We use time-series derived from the FES2014 tidal database in deep water as observations to estimate corrections to the bathymetry. Although the model and estimation algorithm run in parallel, directly applying of DUD would not be affordable computationally. To reduce the computational demand, a coarse-to-fine strategy is proposed by using output from a coarser model to replace the fine model. There are two approaches; One is completely replacing the fine model with a coarser model during calibration (Coarse Calibration) and the second is Coarse Incremental Calibration, that replaces the output increments between the initial model and model with modified parameters by coarser grid model simulations. To further reduce the computation time, the parameter dimension is reduced from $O(10^6)$ to $O(10^2)$ based on sensitivity analysis, which greatly reduces the required number of model simulations and storage. In combination, these methods form an efficient optimization strategy. Experiments show that the accuracy of the tidal representation can be improved significantly at affordable cost. Validation for other time-periods and using coastal tide-gauges shows that the accuracy is improved significantly. However, the calibration period of two weeks is short and leads to some over-fitting of the model.

Plain Language Summary The accuracy of global tide models is currently significantly affected by the gaps in the available bathymetric data, i.e. depth of the ocean, in many regions around the world. At the same time, tides can be measured accurately by satellite radar altimetry. Here, we correct the bathymetry by reducing the disagreement between the model output and observations using mathematical methods. Computational demand for this optimization is large because a single high-resolution model simulation costs much computational time and to optimize the parameters, the model has to be run hundreds of times. We propose two ways to reduce the computational cost. First, we replace the high-resolution model with a lower resolution model being faster but less accurate. This significantly reduces the total computation time. Second, we decrease the number of parameters to an affordable number, by combining the less sensitive parameters into larger areas. Together these two methods form a complete optimization scheme for the estimation of bathymetry and significantly improve the accuracy of the tides computed by the model.

1. Introduction

Coastal flooding poses a serious threat to many people living in coastal zones world-wide. For example, Jongman et al. (2012) estimated that in 2010, 217 million people were living below the 1/100-year exposure line worldwide. This number is expected to grow by about 25% by 2050. Muis et al. (2017) estimated the present day 1/100 year exposure at 158–218 million people. The differences in these last two estimates is caused by two different estimates of the extreme sea levels used in their computations, showing that sea level estimates have a significant impact on the exposure estimates. However, flood defenses can substantially reduce the risks (Hallegatte et al., 2013). Global tide and storm-surge models are very useful tools for estimating flood-risks, including the possible effects of climate change. In addition, these models have many other applications, ranging from providing boundary conditions for coastal models (Zijl et al., 2013) or in the processing of satellite gravity data (Dahle et al., 2019).

© 2021. The Authors.

This is an open access article under the terms of the Creative Commons Attribution-NonCommercial-NoDerivs License, which permits use and distribution in any medium, provided the original work is properly cited, the use is non-commercial and no modifications or adaptations are made.

Global tide models can be classified as (1) purely hydrodynamic forward models, (2) hydrodynamic tide models with data assimilation (Stammer et al., 2014) and (3) empirical tide models. Empirical tide models such as GOT4.8 (Ray, 1999), OSU12 (Fok, 2012), DTU10 (Cheng & Andersen, 2011), and EOT11a (Savcenko & Bosch, 2012) provide tide constituents based on the analysis of data records from satellite altimetry, tide gauges and/or adopted prior models. They can simulate historical tides accurately but most cannot be used for scenario studies. Purely hydrodynamic forward tide models simulate tides based on forcing with the tidal potential without data constraints which can be utilized to study e.g. climate impacts. Hydrodynamic tide models with data constraints are the combination of tidal dynamic equations and data assimilation to improve the model forecast. HAMTIDE (Taguchi et al., 2013), FES2012 (Carrere et al., 2013), and TPXO8 (Egbert & Erofeeva, 2002) are of this type.

Regional storm-surge models are well developed and widespread. Kodaira et al. (2016) developed a global three-dimensional (3D) storm-surge model based on NEMO and showed the potential benefit of including baroclinic processes in the simulation. Arbic et al. (2010) extended a global 3D HYCOM model with tides. These 3D models are computationally quite demanding. Carrère and Lyard (Carrre & Lyard, 2003) developed a two-dimensional (2D) model MOG2D that is used extensively for satellite altimetry. Global Tide and Surge Model (GTSM) (Verlaan et al., 2015) is a 2D combined global tide and surge model developed by Deltares. Although the behavior of tides and surges is quite linear for the deep ocean and steep coasts, there may be significant non-linear interaction between tides and surges on the coastal shelf. Both MOG2D and GTSM use an unstructured grid to apply a higher resolution near the coast where the spatial scales are smaller.

Stammer et al. (2014) compared the accuracy of several assimilative and non-assimilative models and concluded that the assimilative models are clearly more accurate. To be able to apply the model also for different climate scenarios, we will attempt to assimilate observations by estimating several uncertain parameters. Three types of parameters, bathymetry, the bottom friction coefficient, and the internal tides drag coefficient, are considered here. Bathymetry can be measured directly, but until now large parts of the world's oceans remain unsurveyed (Tozer et al., 2019; Weatherall et al., 2015), which creates large uncertainties. Bottom friction and internal tidal friction together determine where the tidal energy is dissipated and are hard to quantify through measurements, though global and regional estimates do exist (Egbert & Ray, 2000).

The research focus in this study is calibration of GTSM for deep ocean because generally tidal propagation scale in deep ocean is larger than it in shallow waters and we assume that once the large scales for deep ocean are properly calibrated the finer details for coastal regions can be refined in later studies. Bathymetry is selected as the first type of parameter to calibrate based on the sensitivity analysis results shown later. A derivative-free calibration algorithm Does not use derivative (DUD), proposed by Ralston and Jennrich (1978) is available in OpenDA software (OpenDA User Documentation, 2016). It is applied to minimize the cost function by comparing the model predictions with data from the FES2014 data set and iteratively computing increasingly accurate estimations of the parameters. Tide gauge data from the University of Hawaii Sea Level Centre (UHSLC) data set is used for the model validation.

Parameter estimation has been applied widely for regional ocean models (Edwards et al., 2015). Das and Lardner (1991) showed the feasibility of estimating parameters for a hydraulic model with periodic tidal observation. Many scientists such as Ten Brummelhuis et al. (1993) and Heemink et al. (2002) investigated the parameter estimation and model validation for the northwest European shelf. Zijl et al. (2013) developed and estimated bathymetry and bottom friction for a tide-surge model (DCSMv6) in this region. Mayo et al. (2014) proposed the use of the Singular Evaluative Interpolated Kalman filter (SEIK) for estimation of Manning's coefficients for an Advanced Circulation (ADCIRC) model. Altaf et al. (2012) applied a Proper Orthogonal Decomposition (POD) based calibration approach to calibrate a large-scale shallow water flow model. Barth et al. (2010) assimilate HF-RADAR current observations with an ensemble smoother to optimize boundary values in the General Estuarine Ocean Model. The sensitivity of barotropic tides to bottom topography and frictional parameters is examined and identified by variational inverse methods(Zaron, 2017). Zaron (2019) further assimilated CryoSat-2 data into a barotropic tide model with a variational approach. Parameter estimation is a promising approach to improve regional tide model accuracy.

However, so far no work on parameter estimation for a global tide and surge model has been reported in the literature. In this study, we developed a parameter estimation scheme for the high-resolution global GTSM.

Compared to regional models, a global model covers a much larger area and does not have open boundaries. As a result of these differences, a global tide model has quite different challenges from regional tide models. One of which is that changes to the bathymetry can have effects very far away from the region of the parameter changes. The high computational complexity and storage usage is also a challenge for the high-resolution global model calibration. On the one hand, computer memory may be insufficient to contain the relevant model output for a long simulation; the memory required increases rapidly with the number of parameters and with the number of observations. On the other hand, computing time is very long for calibration of a high-resolution global model even though parallel processing can be applied. For the DUD optimization algorithm, the computing times are roughly proportional to the number of parameters to be estimated. Thus, the reduction in the number of parameters and reduction in the computing time per model simulation plays an essential role in effective parameter estimation. Therefore, the parameter estimation scheme should be computation-efficient with low computational cost and small memory usage. We improve the computation efficiency of parameter estimation in two key aspects. First, a coarse-to-fine strategy is proposed to replace the model with a coarser grid for parameter estimation. Second, a large reduction in parameter dimension is achieved via sensitivity tests.

In Section 2, the GTSM is introduced. Section 3 describes the parameter estimation scheme, including a description of the observations used, as well as the coarse-to-fine parameter estimation approaches. Section 4 shows the results of the sensitivity analysis for parameter dimension reduction and the parameter estimation results. Validation of the calibrated model is given in Section 5. Finally, the discussion and conclusions follow in Section 6.

2. Global Tide and Surge Model

Water level is modeled in GTSM (Irazoqui Apecechea et al., 2017) by using a version of shallow water equations. Unlike local models that are forced by open boundary conditions, there are no lateral boundaries for GTSM and tides are forced by a tide-generating potential. Some additional physical processes such as self-attraction and loading and internal tidal wave drag are also parameterized because they become relevant in the much larger oceans covered in GTSM than in a regional model. Surge can be simulated by providing additional forces such as wind and air pressure conditions (Verlaan et al., 2015). Therefore, a complete representation of the water level can be provided by GTSM. Long-term water level forecasts for the research of global sea level change becomes possible based on GTSM (Muis et al., 2017).

Although GTSM has been improved continuously over the past few years from version 1.0 to version 3.0, the uncertainties of the model output are still significant and further reduction of these uncertainties would benefit its applications. The main model errors occur in the simplification and parameterization of physical processes, numerical errors and uncertainties of the model parameters. The first two types of errors are studied as part of ongoing modeling efforts. Parameter estimation is an approach to optimizing parameters that cannot be measured directly but does have a major influence on the accuracy of the model output. Parameter estimation is a process, whereby the difference between model results and the measurements is reduced through adjustment of parameters. Here, we build upon the grid and parametrizations of GTSM version 3.0.

2.1. Governing Equations

GTSM is based upon the Delft3D Flexible-Mesh hydrodynamics code (Kernkamp et al., 2011). It uses a version of the vertically integrated or barotropic shallow water equations in two dimensions. The governing equations are:

$$\begin{aligned} \frac{\partial \mathbf{u}}{\partial t} + \frac{1}{h}(\nabla \cdot (hu\mathbf{u}) - \mathbf{u}\nabla \cdot (hu)) + f \times \mathbf{u} \\ = -g\nabla(\zeta - \zeta_{EQ} - \zeta_{SAL}) + \nabla \cdot (\nu(\nabla \mathbf{u} + \nabla \mathbf{u}^T)) + \frac{\tau_b + \tau_{IT} + \tau_s}{\rho h} \\ \frac{\partial h}{\partial t} + \nabla(hu) = 0 \end{aligned} \quad (1)$$

where h is the total water depth, \mathbf{u} represents the depth-averaged horizontal velocity vector, g is the gravitational acceleration, f is the Coriolis force, ρ is the density of water, ν is the horizontal eddy viscosity, ζ is the water level relative to a reference plane, ζ_{EQ} is the equilibrium tide, and ζ_{SAL} refers to the self-attraction and loading effect (SAL), which is a phenomenon with a significant impact on the tidal dynamics especially at the global scale. It describes the effects of self-gravitation attraction and deformation of the ocean floor by the water column on top of it and associated changes on the geo-potential. SAL can change the tide amplitudes by $\sim 10\%$ or more and phases by 30° (Kuhlmann et al., 2011). It can often be excluded in regional models but is a requirement in a global model.

The SAL potential is included in the momentum equation similar to the tidal potential. The SAL term is calculated from the modeled water level at every time-step using a spherical harmonics approach. For a more detailed explanation, see Irazoqui Apecechea et al. (2017).

The terms τ_b , τ_{IT} , and τ_s denote parameterizations of the bottom friction stress, internal tide friction stress, and wind shear stress, respectively. The Chézy quadratic formulation is implemented for bottom friction τ_b (Egbert & Ray, 2000). The form is:

$$\tau_b = -\frac{\rho g}{C^2} \|\mathbf{u}\| \mathbf{u} \quad (2)$$

We use a value of $C = 77(m^{1/2}s^{-1})$. Much of the global energy dissipation occurs through bottom stress in relatively localized regions with shallow water, but ~ 1 TW, which corresponds to 25%–30% of the total global dissipation, occurs in the deep ocean through internal wave drag. Therefore, tidal dissipation through internal wave drag has a great impact on the model and cannot be neglected for an accurate representation of the propagation of waves. In GTSM, it is parameterized as the following equation (Maraldi et al., 2011):

$$\tau_{IT} = -C\rho k^{-1}N(\nabla h \cdot \mathbf{u})\nabla h \quad (3)$$

where C is the dimensionless coefficient, k is typical topography horizontal wave number, N is the depth-averaged Brunt-Väisälä frequency, and ∇h represents the bathymetry gradient. It was computed using data from the Copernicus marine global reanalysis. In our application, $C_{IT} = Ck^{-1}$ is applied as the user-defined coefficient, with the value of 0.015. It was based on a global estimate of internal tide dissipation and reproduction of tides by the model.

Although this study focuses on modeling tides, the model is often applied as a combined model for tides and surge. If so, the influence of atmospheric pressure and wind-drag is added to the model forcing (Pugh & Woodworth, 2014). Meteorological forcings are then applied as time and space varying wind and air pressure. The wind stress is modeled as the following equation:

$$\tau_s = \rho_a C_d \|\mathbf{u}_{10}\| \mathbf{u}_{10} \quad (4)$$

where ρ_a is the density of air, and \mathbf{u}_{10} is the term of the wind speed 10 meters above the free surface. In the Charnock formulation (Charnock, 1955), the wind drag coefficient C_d is dependent on the wind speed \mathbf{u}_{10} and a user-defined Charnock constant to represent the surface roughness, which is 0.041 in our model.

2.2. Bathymetry

One of the most important parameters in tide modeling is bathymetry. In GTSM the bathymetry is derived from the global products General Bathymetric Chart of the Oceans data set (GEBCO 2019). GEBCO is continually developing its bathymetry datasets to improve the accuracy and the coverage of measured ocean

depth. In Section 4.2 we compare two versions of bathymetry (GEBCO 2014 and GEBCO 2019 data sets) and their impact on model performance. They are projected to the unstructured grid by means of interpolation. GEBCO 2019 provides global coverage on 15 arc-second resolution with measured and estimated seafloor topography. For Europe, the EMODnet data set with a resolution of about 250 m is used to overwrite the bathymetry in those regions where there are regional samples. GTSM uses Mean Sea level (MSL) as its vertical reference. All bathymetric data is assumed to be relative to the Lowest Astronomical Tide (LAT). Therefore, a correction is applied for the LAT-MSL difference. However, even though the techniques developed in the submarine survey and depth are updated regularly, there is still a lack of data for bathymetry at a global scale. This has a significant impact on the tide reproduction, as we will show later.

2.3. Computational Grid

The amplitudes of the coastal tidal components are normally larger than that in the deep sea while the wavelengths are typically smaller. To model this accurately a high resolution is required in coastal areas, which may lead to a large computational cost. Here we make use of an unstructured mesh with triangles and quadrilaterals, which makes it possible to provide a much higher resolution in coastal areas and lower resolution in the deep ocean to maintain an acceptable computational cost (Kernkamp et al., 2011). Compared to the regular latitude-longitude grid, there are two advantages of the unstructured mesh. First, grids in high latitudes are thinned to reduce the requirement of computing resources. And second, some areas that require high resolution, such as coastal areas and continental shelves where much of the dissipation occurs, can be refined.

Two different versions of GTSMv3.0 with two resolutions have been developed (GTSM with the coarse grid and GTSM with the fine grid hereinafter). GTSM with the coarse grid has a resolution of ~50 km in the deep ocean and 5 km in the area near the coast. The largest grid cells in the fine version of GTSM are 25 km. In the coastal area, the resolution is 1.25 km in Europe and 2.5 km along coasts elsewhere. The number of grid cells is ~4.9 million and the coarse version has about 2 million cells.

As a result of an efficient semi-implicit discretization, the computational cost of the model simulation is reduced. However, a model simulation with the GTSM with the fine grid for a period of 45 days still takes approximately 10 h on a computer with 20 cores, consisting of 5 Intel E3 processors with four cores each, and 3 h for the same simulation for the coarse model. To reduce the single model computational time, we moved the computations to the Dutch National Supercomputer Cartesius, where the running time for the same simulation on 200 cores reduced to 70 min for the fine model and 25 min for the coarse model. For individual runs this computing time is acceptable, but for parameter estimation which requires hundreds of simulations, this results in running times of weeks. Therefore, an effective parameter estimation scheme should be designed.

3. Parameter Estimation Framework

3.1. Observations Network

The datasets applied for parameter estimation and validation in this study are deep ocean tides from the FES2014 data set and the tide gauge data from the UHSLC (Caldwell & Thompson, 2015).

The FES2014 data set was produced by Noveltis, Legos, and CLS and distributed by Aviso+, with support from CNES (<https://www.aviso.altimetry.fr/>). It comes from the FES (Finite Element Solution) tide model with the assimilation of satellite altimeter data. The output of some models with and without data assimilation is compared by Stammer et al. (2014), FES2012 showed excellent accuracy when compared with tide gauge and satellite altimeter data. FES2014 is the updated version of FES2012. The main advantage of using a tidal database such as FES2014 for our deep ocean calibration is that a tide time series can be obtained for arbitrary time periods globally. With direct use of satellite altimetry one would have to cover a much longer time span, due to the relatively long repeat cycle, e.g. 12 days for Sentinel 1. We generated 1973 time series from the FES2014 data set with 32 tide constituents (excluding long-term constituents SA and SSA) for the calibration of bathymetry in January 2014 with a 10-min time step. First, 3,000 equally spaced points on a sphere were generated using Fibonacci and latitude-longitude lattices (González, 2009), and then we

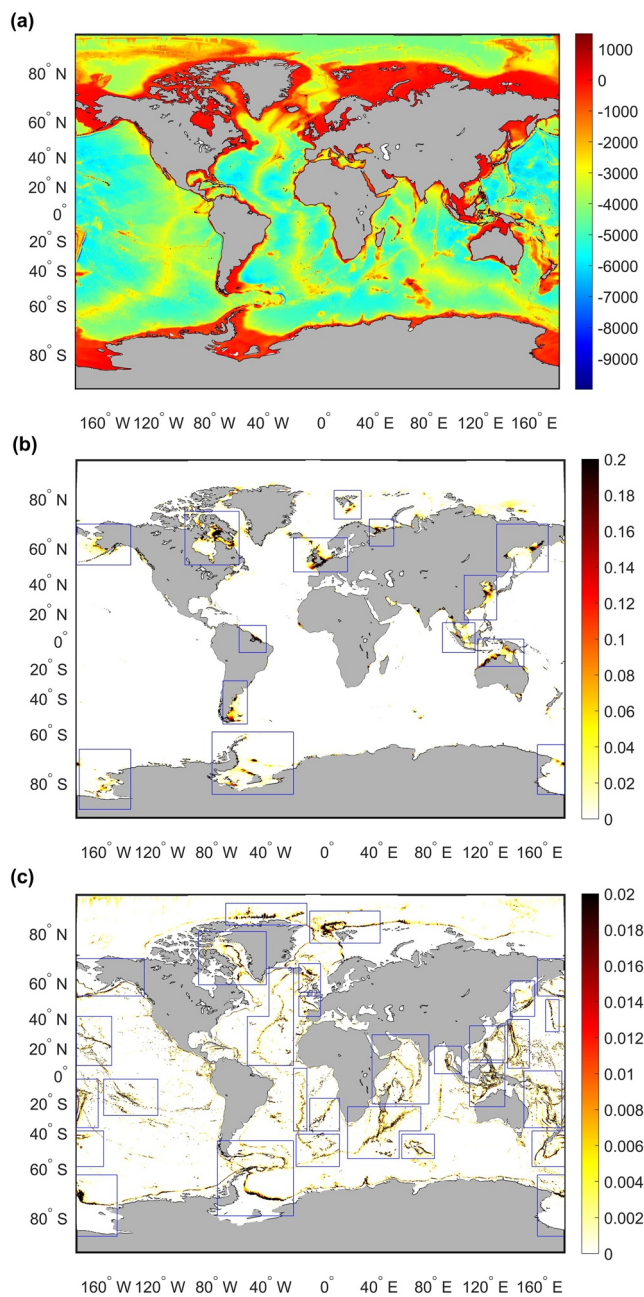


Figure 1. Spatial distribution of uncertain parameters: (a) bathymetry distribution in global oceans (unit:m); (b) tide energy dissipation by bottom friction (unit: W/m^2); (c) tide energy dissipation by internal tide friction (unit: W/m^2). The areas with large tidal energy dissipation are shown in the areas with blue boxes.

the difference between the model output and the FES2014 data set. The sensitivity is computed as the relative change of the cost function with respect to each perturbed parameter. The model output with perturbed bathymetry shows much larger changes than that with the perturbed internal tide drag coefficient, which means that GTSM is more sensitive to bathymetry than to internal tide friction and bed friction. Therefore, bathymetry is the only type of parameter we selected to estimate for GTSM in this paper.

removed the locations on land and in shallow waters, which finally results in 1973 locations for deep ocean. The details of the observation locations are shown in Section 4.3.

The UHSLC has a global collection of ~500 tide gauge time series. The availability of data varies over the years, with the amount of locations increasing over time, except for the few most recent years. We retrieved the 283 tide gauge series that are available from the hourly research quality data set in the year 2014. The tide analysis was performed with the tidal analysis software TIDEGUI. First, we separate tide and surge from the measured water level, since our model calibration is based on the tide representation only. Second, because the simulation time window for the parameter estimation covers only a short time period, the (solar) annual and semiannual constituents SA and SSA were removed after the tide analysis. We obtained a set of 93 harmonic constituents. After that, the tide and surge representations were visually inspected in comparison to the measured series in the tide analysis procedure. The distribution of the locations is somewhat irregular and most locations are in coastal areas.

Even though the FES2014 data set has assimilated tide gauge data, the UHSLC data set can still be seen as independent from our calibration because the FES data used for calibration was limited to deep water, while almost all tide gauges are at the coast. The purpose of using UHSLC data is to study the impact of the calibration in the coastal areas.

3.2. Optimization of Model Parameters

To calibrate GTSM, we attempt to estimate parameters first in global deep ocean waters and then later in shallow water areas. The three most uncertain parameters in a global tide model are bathymetry (shown in Figure 1a), energy dissipation by bed friction (Figure 1b) and internal tides (Figure 1c). The blue boxes show the regions with high levels of tide energy dissipation. All of the boxes in Figure 1b of bottom friction are in the coastal areas, which makes the model very sensitive to resolution in these regions. Tide energy dissipation through internal tides friction is globally distributed and related to the bathymetry change, especially in the mid-ocean ridges and trenches, continental shelves, and island chains. Therefore, we aim to split the calibration into two stages. The first is calibration at the large scales in the deep ocean and the second is refine the coastal regions with more measurements included locally. In this paper, we focus on the first stage deep-ocean calibration.

Selecting only the dominating parameter in the model and ignoring others can be an effective way to reduce the parameter dimensions. A simple sensitivity experiment is performed to compare the influence of bathymetry and internal tides drag coefficient on the GTSM. The global oceans are divided into seven regions, GTSM is simulated with 5% perturbation for the bathymetry and 20% perturbation for internal tides drag coefficient in each region. Cost function is defined as the sum of the squares of

3.3. Parameter Estimation Algorithm

Parameter uncertainty can be reduced via optimization techniques to tune the model output toward the data. Here we use an algorithm called DUD, since it is the default algorithm in the generic data-assimilation toolbox OpenDA and there is a lot of experience with this method. DUD is an algorithm similar to Gauss-Newton algorithm but with a derivative-free method to solve non-linear least squares problems. The algorithm will attempt to minimize a cost function in an iterative manner. In addition to an observation term, the cost function also contains a weak-constraint or background term in order to constrain changes compared to the initial parameters where the fit to observations does not improve significantly. In the brief description of the DUD algorithm below, the cost function is limited to the observation term only, to keep the description concise. The observation term $J_o(x)$ in the cost function measures the difference between the model output and observations in a time range $t \in [t_1, t_k]$, which is:

$$J_o(x) = \frac{1}{2} [y - H(x)]^T R^{-1} [y - H(x)] \quad (5)$$

where y is the field observation vector including all times $t \in [t_1, t_{N_t}]$ and stations $(1, \dots, N_s)$, and the term x is the parameter vector with the number n . $H(x)$ is the model output matching the observation locations and times and R is the observation error covariance. The dimension of y and $H(x)$ is $O(N_s N_t)$. The minimization processes are performed with the following steps:

1. Obtain model output $H(x_i)$ with the first guess for all parameters $x_0 = x_b$, as well as n runs each with one perturbed parameter ($x_1 = x_b + \delta e_1, \dots, x_n = x_b + \delta e_n$).
2. Calculate the cost function $J_o(x_i)$, $i = 0, \dots, n$ for the $n + 1$ simulations.
3. Perform the iterations of the minimization process.
 - (1) Reorder the cost function values from the largest value to the smallest as $J_o(x_0) \geq J_o(x_1) \geq \dots \geq J_o(x_n)$.
 - (2) Create an approximate linear model by interpolation between the $n + 1$ model predictions already computed. The linearization equation is:

$$H(x) \approx H(x_n) + M\Delta(x - x_n) \quad (6)$$

with $M = FP^{-1}$, where the i th column of F and P are $F_i = H(x_i) - H(x_n)$, $P_i = x_i - x_n$

- (3) Solve the linear problem and update the new parameters by:

$$x_* = x_n + [M^T M]^{-1} M^T [y - H(x_n)] \quad (7)$$

- (4) If $J_o(x_*) < J_o(x_n)$, update the parameters and cost function set by using x_* to replace x_0 which has the highest cost function, i.e. we keep the $n + 1$ best estimates.
- (5) Otherwise, do a line search until the cost function is improved. Update the parameters in the same way as shown in (4).
4. Check the termination criteria in steps (4) and (5); if the results do not satisfy any one of the criteria, then return to step 3 (1), otherwise stop the iterations.

Several constraints are imposed to make the correction factors realistic. One is the weak constraint applied as a background term in the cost function which will reduce the parameter adjustments when the fit to the observations does not improve significantly. Another is we added a hard constraint to all the parameters by limiting changes to 10%. This is because the initial number of simulations in step 1 is $n + 1$ and the dimension of matrix M is $N_s N_t \times n$. The computational time increases proportionally to the number of model simulations and running time for each simulation. The parameter dimension has a major impact on the number of simulations and a higher model resolution also increases the computational time for each model simulation. It results in the memory required to store the matrix M ultimately turning out to be a limiting factor in our application. Therefore, we propose two further approximations to speed up the computations and limit the use of memory. First, we propose a coarse-to-fine parameter estimation scheme to reduce the computational time for each simulation in Section 3.4. Second, the parameter dimension is reduced to an acceptable scale by sensitivity analysis, which will be introduced in Section 4.2.

3.4. Coarse-to-Fine Parameter Estimation

In this section, two approaches for the coarse-to-fine parameter estimation strategy are proposed that replace part of the simulations with the fine grid GTSM by simulations with a coarser grid. The estimated parameters for the coarse model are reused for the fine model. Two possible approaches are:

1. Approach 1: Coarse Calibration, which completely replaces the fine model with a coarser grid model during the calibration
2. Approach 2: Coarse Incremental Calibration, which replaces the increments between the output from the initial model and the model with modified bathymetry using a coarser grid. The bias between the coarse model and the fine model is corrected for

The cost function for Approach 1 is:

$$J_1(x) = \frac{1}{2}[y - H_f(x)]^T R^{-1}[y - H_f(x)] \quad (8)$$

where the term $H_f(x)$ and $H_c(x)$ are the model output of the fine and coarse resolution, respectively. In Approach 1, the model simulation runs only on the coarse grid, which results in a large reduction in computational time. However, the minimization of the cost function only involves the coarse model without any direct relationship to the fine model. Since a coarser model is in general less accurate this will lead to a compensation for these errors in the parameter estimates, which still apply to the fine model.

Therefore, we also propose a second approach (Approach 2: Coarse Incremental Calibration) that only replaces the difference between the initial output and the adjusted model output of the fine model ($\delta H_f = H_f(x) - H_f(x_b)$) by a coarser grid ($\delta H_c = H_c(x) - H_c(x_b)$). It is similar to the incremental formula to reduce the computational cost of 4D-Var, which is widely used in the implementation of data assimilation for the ECMWF weather model (Courtier et al., 1994).

Our experiment shows that the difference between increments δH_f and δH_c is on average small compared to the RMS of δH_f and δH_c , 0.68 cm compared to 3.26 cm (not shown here). Therefore, the fine grid increments in most regions are well represented by the coarse grid. We assume $\delta H_f \approx \delta H_c$, and thus the new cost function is generated as:

$$J_2(x) = \frac{1}{2}[y - H_f(x_b) + H_c(x_b) - H_c(x)]^T R^{-1}[y - H_f(x_b) + H_c(x_b) - H_c(x)] \quad (9)$$

The new cost function for initial simulation in Approach 2 represents the disagreement between the observations and the fine model predictions. Compared to Approach 1, the new cost function gives a better description of the initial fine model. The computational times of these two approaches are reduced and are almost the same since only one more simulation of the fine model is required in Approach 2. After the estimation, the correction factors of bathymetry are interpolated to the fine model's unstructured grid before simulations with the fine grid.

4. Numerical Experiments and Results

This section first provides more detail on how the calibration was performed. Next, it explains how we reduced the number of parameters to make the computation times and memory usage manageable. Finally, it describes the results from the calibration experiments.

4.1. Experiment Set-Up

As discussed in Section 3.1, the accuracy of the model will be expressed relative to time-series computed from FES2014. Direct use of altimeter data to calibrate the model would require a simulation covering at least several years, which is not feasible computationally in this context. In our experience, time-series from tide gauges should cover between a month and a year to obtain accurate tidal estimates. Unfortunately, it turned out that this did not fit into the memory (32Gb) on our cluster. One spring-neap cycle, of about half

Table 1

Regional RMSE, Bias, and SD Between Model Predictions With Different Bathymetry for Two Resolutions and the FES2014 Data in (cm) From January 1 to 14, 2014

Model	GTSM with the coarse grid						GTSM with the fine grid					
	GEBCO 2014			GEBCO 2019			GEBCO 2014			GEBCO 2019		
Bathymetry	RMSE	Bias	SD	RMSE	Bias	SD	RMSE	Bias	SD	RMSE	Bias	SD
Region												
Arctic Ocean	7.03	0.37	7.02	7.06	0.44	7.04	5.25	0.41	5.22	5.24	0.65	5.18
Indian Ocean	7.94	-0.06	7.94	6.70	-0.11	6.70	6.51	-0.05	6.51	5.57	-0.10	5.57
North Atlantic	8.9	-0.02	8.96	6.89	0.01	6.87	7.89	0.03	7.89	5.41	0.07	5.41
North Pacific	7.41	-0.13	7.41	6.97	-0.12	6.96	6.03	-0.09	6.02	5.69	-0.07	5.69
South Atlantic	5.45	-0.22	5.45	4.76	-0.22	4.76	4.68	-0.20	4.67	4.15	-0.23	4.14
South Pacific	7.59	-0.20	7.58	7.03	-0.21	7.03	5.81	-0.19	5.80	5.57	-0.25	5.56
Southern Ocean	5.86	0.01	5.86	5.35	-0.02	5.34	4.47	-0.09	4.47	4.28	-0.13	4.27
Total	7.28	-0.09	7.27	6.47	-0.10	6.46	5.88	-0.09	5.88	5.23	-0.11	5.22

GTSM, Global Tide and Surge Model; RMSE, root mean square error; SD, standard deviation.

a month, did fit into the memory and was selected as the best feasible option at this point. The tidal potential used in the model accounts for the tide components with a Doodson number ranging from 57.565 to 375.575. The minimum threshold for the amplitude of the tidal spherical harmonic is 0.03 m, which results in a set of 58 tidal generating frequencies. Long-period tide constituents SSA and SA are excluded from the model output and observations, because long-period tides are affected by non-gravitational influences. From the tidal constituents in FES2014 the time-span is not limited to a particular period. Therefore, we selected January 2014, when the most tide gauges were available for validation.

The simulation time is chosen from January 1 to 14, 2014 and the spin-up time for the model is from two weeks before 1 January to make sure that the initial values (zeros) for the sea level and currents no longer have a significant impact on the results. Each time-series, with a time-step of 10 min thus has a length of $N_t = 2,016$. In total $N_s = 1,973$ locations were selected, resulting in an output of $N_s * N_t = 3977568$ values per simulation.

4.2. Sensitivity Analysis and Parameter Dimension Reduction

In order to obtain a better initial bathymetry input for GTSM, a comparison of model simulations with bathymetry input from GEBCO release 2014 and GEBCO 2019 was performed.

Table 1 shows the Root Mean Square Error (RMSE) bias difference and standard deviation (SD) for the two grid resolutions and two bathymetry inputs against the time series from FES2014 for seven regions from January 1 to 14, 2014. The bias difference between the model output and observations is very small with the maximum value at the millimeter level. It illustrates that the tides computed with the fine grid are more accurate than for the coarse grid using the same bathymetry source from both RMSE and SD comparisons. Moreover, the model output with GEBCO 2019 bathymetry is more accurate than that with GEBCO 2014. This shows that reducing the uncertainty of bathymetry can significantly improve the model performance. Based on these experiments, we selected GEBCO 2019 as the source for the initial bathymetry.

In principle the bathymetry can be different in every grid node of the model. However, it would be computationally infeasible to treat the bathymetry at every grid node as a degree of freedom in the estimation. Moreover, the content of the information contained in the observations is not enough to estimate so many parameters.

Thus, we attempt to reduce the number of parameters and use a single value to adjust the bathymetry with one correction factor per spatial region S_i , $i = 1, \dots, n$. For every grid node j in the spatial region we adjust the parameter from D_j to D_j^* according to:

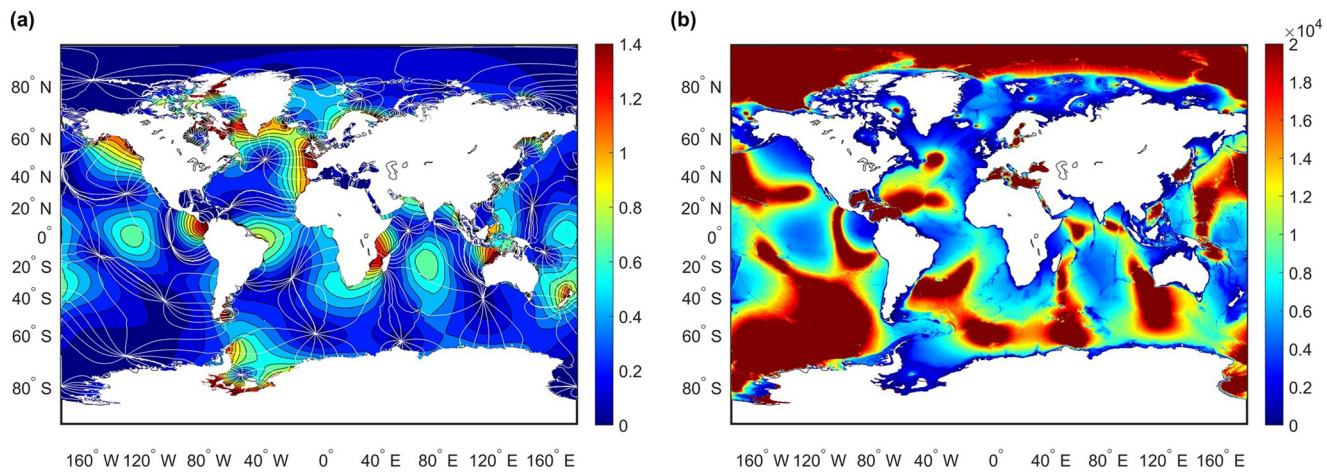


Figure 2. (a) Amplitude and cophase lines of M_2 constituent (m); (b) propagation length based on perturbed bathymetry with M_2 constituent (km).

$$D_j^* = (1 + [x]_i)D_j \text{ for } j \in S_i \quad (10)$$

where $[x]_i$ is the i^{th} element of the reduced parameter vector x and we use the initial estimate $x_b = 0$ (a vector with n zeroes). For instance, if $[x]_1 = 0.10$, the depth in region S_1 will be increased by 10%. In GTSM the number of grid nodes is $O(10^6)$, while the feasible number of independent parameters during the estimation is $O(10^2)$. Thus, we would like to design $O(10^2)$ regions or sub-domains where the response of the model is expected to be similar and the sum of the sensitivities between the regions is of similar magnitude.

Let us first define the sensitivity s_i with respect to region S_i as

$$s_i = \frac{J(x_b + \delta e_i) - J(x_b)}{J(x_b)} \quad (11)$$

which is the relative change in cost function when changing the parameter (here bathymetry) only in the i^{th} region by multiplication with a factor $1 + \delta$.

4.2.1. Spatial Scale

Before the final selection of sub-domains for calibration, we first attempt to create a rough estimate of the spatial length-scale at which one can estimate the bathymetry from the available tidal data. Consider for example the constituent M_2 , which is dominant in many places around the world. Figure 2a gives an impression of the amplitude of M_2 around our planet. The largest amplitudes are often in coastal areas. The color scale is limited to 1.4 m, but there are a few regions where the amplitude is larger. Now consider the following thought experiment. When the tide propagates from one location to another, a perturbation of the bathymetry between these positions could lead to a water level difference. The water level that arrives by propagation with speed c from a position at distance l to it can be described as:

$$H(t) = A \cos\left(\omega\left(t - \frac{l}{c}\right)\right) \quad (12)$$

where l is the propagation length, A and ω denote the amplitude and the frequency of M_2 constituent respectively. $H(t)$ is the water level at time t . If the bathymetry is perturbed between these points, this will affect the propagation speed $c = \sqrt{gD}$ and the difference of M_2 tide will be:

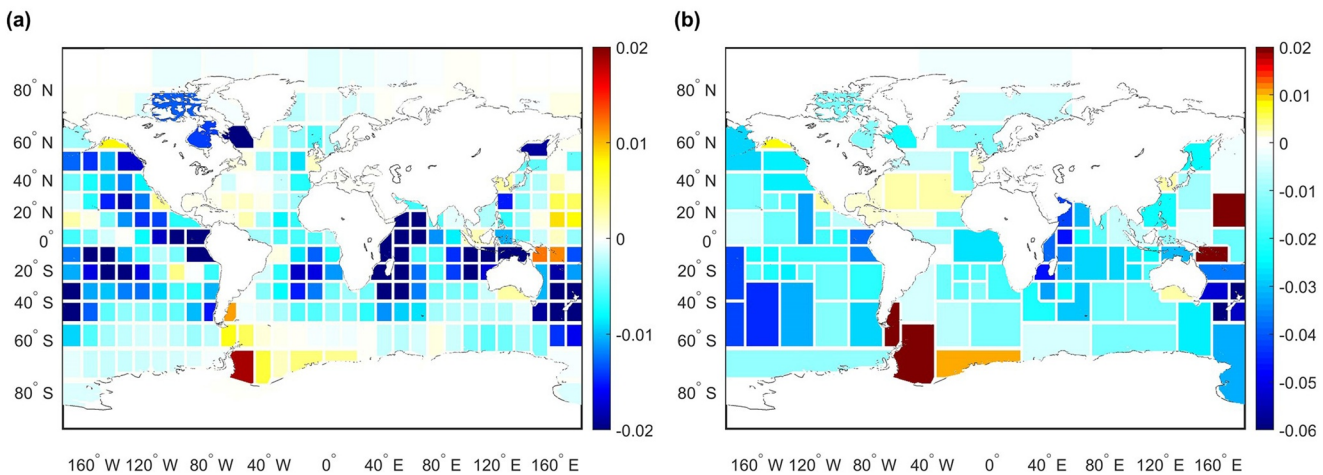


Figure 3. Bathymetry sensitivity test in GTSM with the coarse grid: (a) bathymetry perturbation is applied in 285 sub-domains; (b) bathymetry perturbation is applied in 110 sub-domains. GTSM, Global Tide and Surge Model.

$$\Delta H(t) \approx A \sin\left(\omega\left(t - \frac{l}{c}\right)\right) \frac{\omega l g \Delta D}{2c^3} \quad (13)$$

To really observe this difference, the change in tide should be larger than the noise in the measurements. Thus for observations with noise σ (standard derivation) one can give a minimum length scale over which changes in bathymetry $\Delta D = \alpha D$ may become visible in the observations:

$$l_c = \frac{2\sigma c^3}{A\omega g \Delta D} = \frac{2\sigma \sqrt{gD}}{\alpha A \omega} \quad (14)$$

The propagation length-scale l_c is inversely proportional to the M_2 amplitude and proportional to the square-root of the depth. It is expected that a small M_2 amplitude and a large value of bathymetry lead to a long propagation length and weak sensitivity. Figure 2b provides an overview of propagation length at the global scale with $\sigma = 0.05$ m and 10% perturbation of bathymetry. Small values of propagation length illustrate the larger sensitivity of bathymetry corresponding to M_2 constituents. From this figure, one can conclude that it is probably difficult to estimate the bathymetry corrections for the Arctic and parts of the interior of many oceans, while conditions are much more favorable along the coasts and in shallow areas. The values of l_c should not be taken too literally, since the underlying formulas are only a rough approximation of the dynamics and the estimates for measurement noise and bathymetric uncertainty can be debated. Still, the method nicely illustrates the large differences in potential spatial resolution for estimating bathymetry from tides.

4.2.2. Sensitivity Experiment

We generate 285 $10^\circ \times 10^\circ$ sub-domains based on the estimates of propagation length being larger than 10° in most of the oceans. Figure 3a shows the sensitivity results in these sub-domains according to Equation 11 with FES2014 tide data. Many sensitive sub-domains are in the coastal areas or regions with a large M_2 amplitude. The sensitivity in all regions is smaller than 2%. Some regions such as the Arctic Ocean have very small sensitivity values. The number of 285 sub-domains is too large for our computational resources, so we merged some neighboring sub-domains to reduce the parameter dimension and CPU times. Neighboring sub-domains are aggregated if they satisfy both criteria: (1) they have the same sensitivity directions (both negative or both positive) and (2) their propagation lengths are large and the sensitivity is small. Correction factor of bathymetry in each sub-domain is applied for every grid cell. A two-degree transition area is applied between neighboring regions. The correction factors in the cell of the transition areas is interpolated by the model, using linear interpolation on a triangulated discretization with the samples defined in the

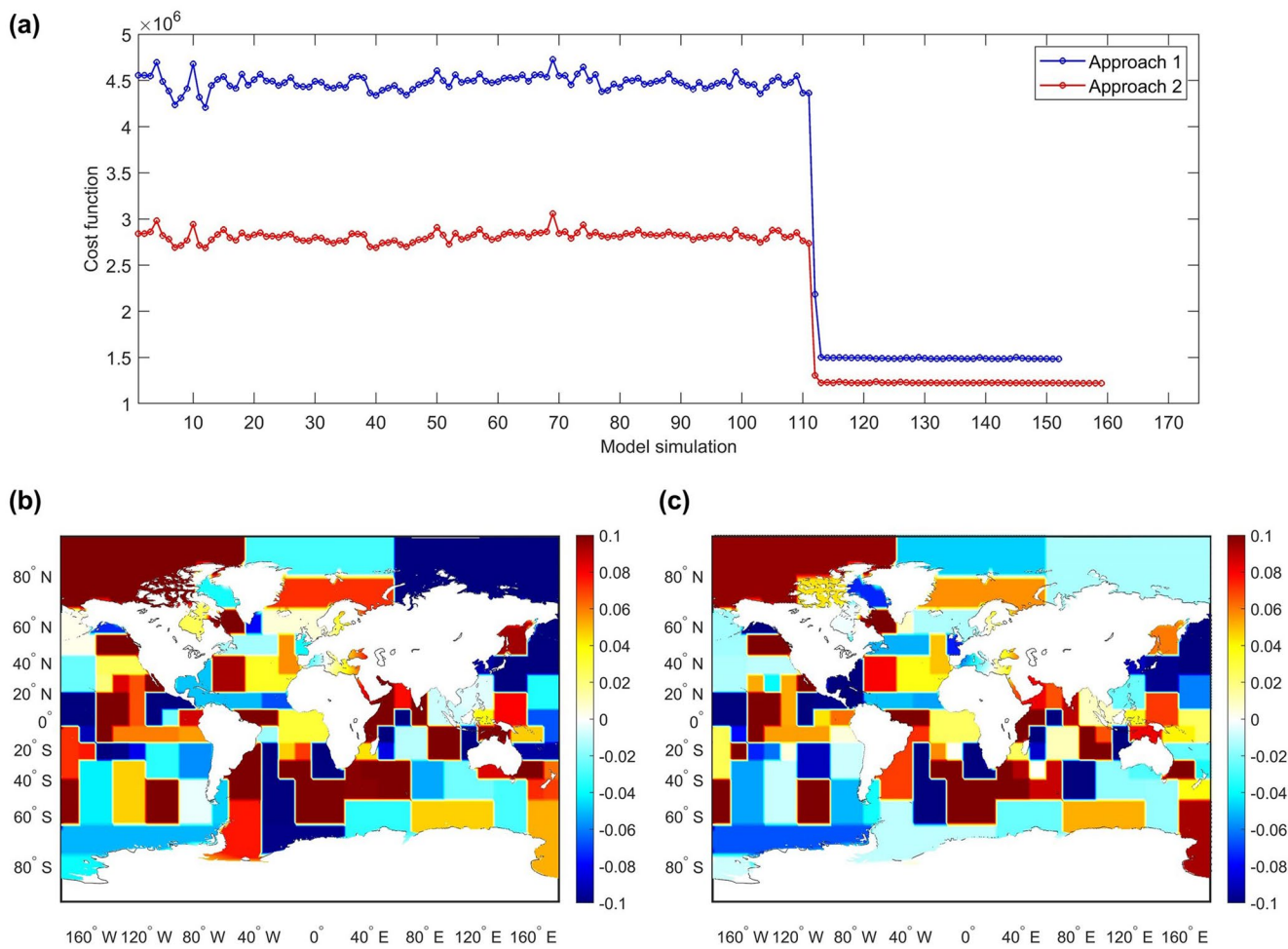


Figure 4. (a) Cost function for two approaches; Bathymetry differences in Approach 1 (b) and Approach 2 (c) show the value of (x) in Equation 10.

calibration as nodes. The sensitivity analysis results for these 110 aggregated sub-domains are reported in the right-hand panel of Figure 3. The values of sensitivity are between -0.06 and 0.02 . As a result, the parameter dimension has been reduced from $O(10^6)$ originally to 110 through the sensitivity analysis. Also, the size of the matrix H is 110×3977568 which is now small enough to deal with, given the constraint of limited computer memory space.

4.3. Parameter Estimation Results

We apply the coarse-to-fine parameter estimation method as described in Section 3.4 with 110 sub-domains. Figure 4a illustrates the cost function in each iteration for parameter estimation for the two approaches. It is not easy to observe the difference between the estimated and initial bathymetry from the map. So, we show the final relative change to the bathymetry in Figures 4b and 4c, which is the correction factor $[x]$ in Equation 10. The final bathymetry estimated by the two approaches has a similar distribution.

In Figure 4a, the first 111 iterations are running with perturbed parameters and the result of each of these simulations is independent from each other. After the perturbed simulations, new parameters are iterative estimates based on the previous model output. Therefore, these first 111 simulations can be computed in parallel if enough computing resources are available, after that parallelization has to be sought within a single iteration. The computational cost of the two approaches is similar and Approach 2 required seven more iterations than Approach 1. This is a relatively small difference and could be different with slightly different settings. We compared the values of the cost function of the original GTSM model with two resolutions

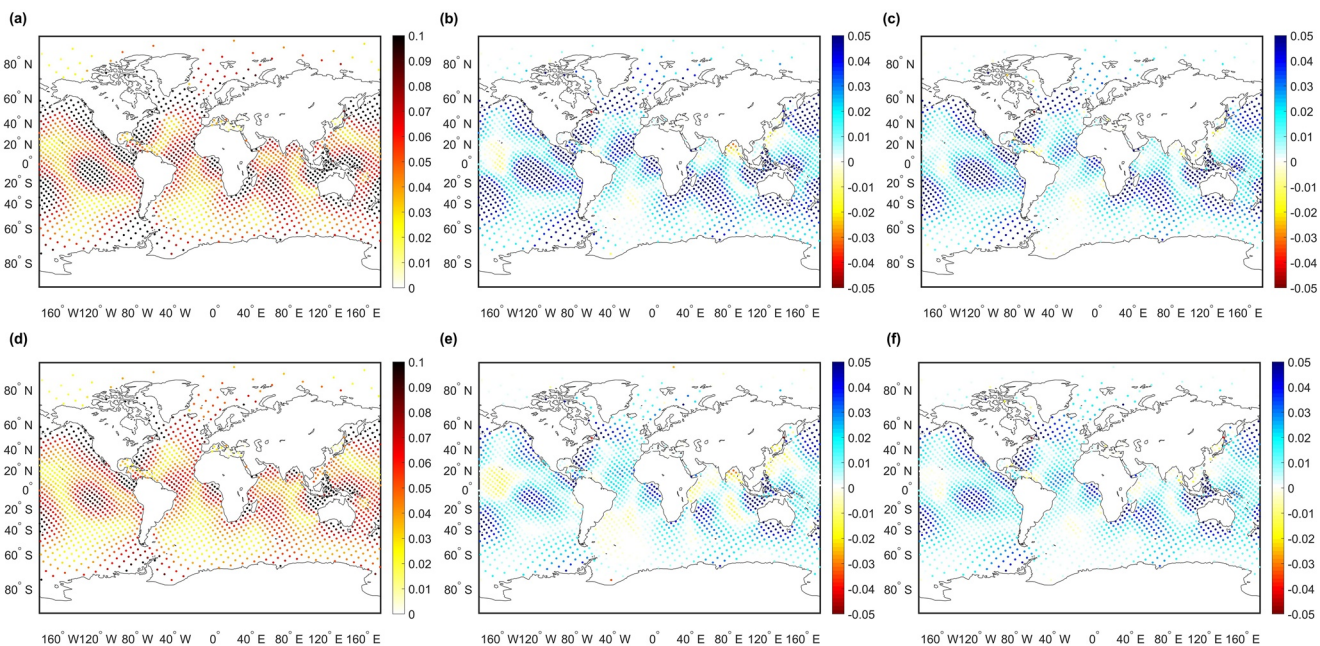


Figure 5. Spatial distribution of RMSE for two approaches from January 1 to 14, 2014. The upper panels depict the results for GTSM with the coarse grid and the lower panels are for the fine grid model. (a) and (d) RMSE for initial model; (b) and (e) difference in RMSE between the initial and estimated model in Approaches 1; (e) and (f) RMSE difference in approaches 2. The color blue indicates improvement (unit: m). GTSM, Global Tide and Surge Model; RMSE, root mean square error.

and FES2014 observations. It is expected that the cost function value of Approach 2 is smaller than that of Approach 1. The values of the cost functions are greatly reduced from 4.56×10^6 to 1.48×10^6 in Approach 1 and from 2.84×10^6 to 1.22×10^6 in Approach 2. The percentage of reduction is approximately 67.5% for Approach 1% and 57% for Approach 2. The cost functions of both approaches show similar behavior with a sharp reduction in the first few estimation iterations and little improvement after that. It should be noted that the lower final cost function value of Approach 2 does not necessarily imply a higher accuracy of the estimated model output, since the methods do not use the same cost function. The cost function in Approach 1, as shown in Equation 8 only includes the coarse grid model results while the cost function in Approach 2 (Equation 9) also includes the initial output from the coarse and fine grid models. Therefore, the cost functions for these two approaches cannot be compared directly and we use the RMSE for comparison instead.

Figure 5 shows the RMSE for the final model simulation with the estimated bathymetry as input from 1–14 January 2014. Before the parameter estimation, GTSM with the fine grid (Figure 5d) has better performance than the coarse grid model (Figure 5a) almost everywhere. The RMSE difference between the model with and without estimation are shown in Figures 5b and 5c (coarse model) and Figures 5e and 5f (fine grid). The results in Figures 5b and 5e are for Approach 1, and Figures 5c and 5f are for Approach 2.

It can be observed that compared to FES2014 “observations,” the estimated model output in most areas has improved significantly. The two approaches show a similar spatial pattern of RMSE. There are also a few areas where the RMSE values are marginally higher than the initial model; see the areas in yellow or red in Figures 5b, 5c, 5e, and 5f (negative values in the RMSE difference mean the estimated results are worse than the initial results). The most persistent area, with consistently the worst results, between the experiments seems to be in the Bay of Bengal. Perhaps, effects other than bathymetry, play a role here, such as a lack of resolution around the large river delta in the north. In summary, we conclude that the estimated model has improved significantly on the global scale.

A comparison of spatially averaged RMSE over seven regions for two approaches, the coarse model and the fine model, are shown in Table 2.4. Compared to the initial model output, the accuracy of output after optimization of both the fine and coarse models are improved in every region. For instance, the RMSE has

Table 2*Regional RMSE After Bathymetry Estimation in GTSM With Two Resolutions in (cm) From January 1 to 14, 2014*

RMSE	GTSM with coarse grid			GTSM with fine grid		
	Initial	Approach 1	Approach 2	Initial	Approach 1	Approach 2
Arctic Ocean	7.06	4.55	5.78	5.24	3.98	4.34
Indian Ocean	6.70	3.74	3.89	5.57	4.21	3.62
North Atlantic	6.89	3.90	4.51	5.41	3.47	3.43
South Atlantic	6.97	4.44	4.69	5.69	4.40	3.96
North Pacific	4.76	3.16	3.65	4.15	3.32	3.11
South Pacific	7.03	3.62	4.16	5.57	3.73	3.43
Southern Ocean	5.35	3.16	3.69	4.28	3.04	2.97
Total	6.47	3.76	4.19	5.23	3.78	3.49

GTSM, Global Tide and Surge Model; RMSE, root mean square error

a reduction of 42% and 35% for the model with coarse grid in Approaches 1 and 2, respectively, and, in the fine model, it is also reduced by 28% and 33%, respectively.

Because the coarse model Approach 1 directly optimizes the mean RMSE, so one would expect an improvement. For Approach 2, the cost function used for optimization uses observations that are corrected for differences between the fine and coarse models. Still, Approach 2 improves the performance for all regions compared to the initial model. Finally, both approaches improve the accuracy of the fine model, even though the fine model is already more accurate than the coarse model initially. On average, the fine model with the calibrated bathymetry of Approach 1 has an accuracy similar to the coarse model for Approach 1. Thus, it does not really benefit from the higher initial accuracy of the fine model. However, Approach 2 does benefit from the higher initial accuracy of the fine model and results in the best performance of all the combinations for the calibration time span. Most regions behave similar to the average, but in the Arctic Approach 1 results in a better fit to the data, than Approach 2.

In summary, both calibrations result in an improved fit to the measurements for both the coarse and the fine model. For the coarse model Approach 1 seems slightly better and for the fine model Approach 2. This is of course comparing to the same data as was used for the estimation. Compared to Approach 1 with only the coarse grid estimation, Approach 2 uses both coarse and fine grid models in the cost function. Approach 2 probably has the advantage to capture some small-scale features independently of the coarser grid. The aim is that for Approach 2 the estimation results are more accurate for the fine grid GTSM.

5. Model Validation

In order to validate the model performance more independently from the simulation period and data that we used in the estimation stage, the forecast has been compared against the FES2014 data for the whole of the year 2014. Also, the main tide component M_2 is analyzed with FES2014 data. In addition, the model forecast is also compared to a large number of tide gauges for both tide and surge validation.

5.1. Validation with FES2014 Data Set

The whole of the year 2014 is chosen as the validation period with the FES2014 data set to analyze the model performance. Two-time period are used as examples for detailed model performance explanation. The first period is chosen from January 15 to 31, 2014, which are the days in January following the estimation stage and this contains the second spring-neap cycle within the first lunar cycle in 2014. The model forecast on July 1–31, 2014 is also analyzed here to inspect the model performance in another season.

Figure 6 shows the forecast regional RMSE of the fine resolution GTSM with estimated bathymetry by the two approaches in the 12 months of the year 2014. RMSE for all the seven regions has improved significant-

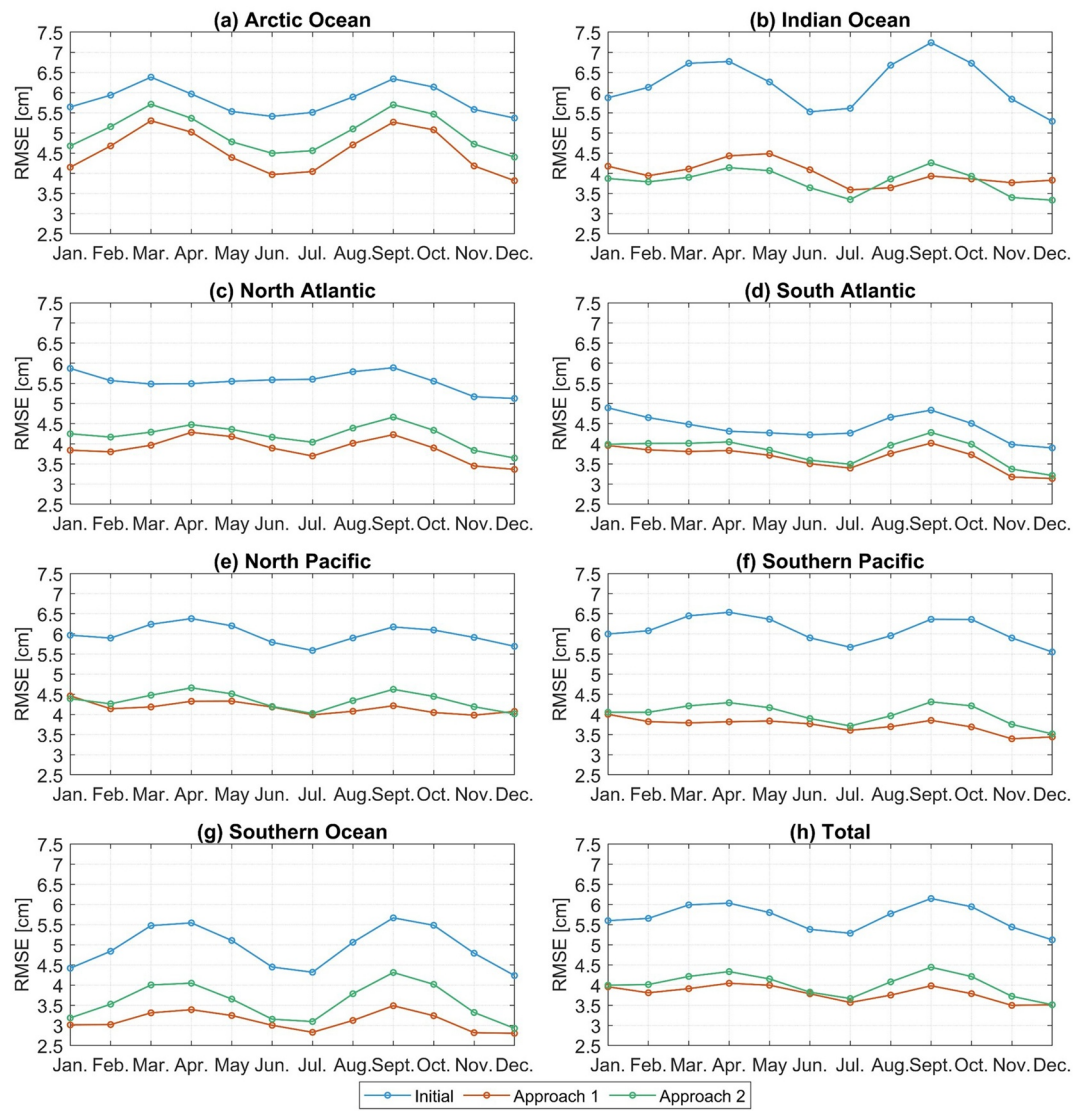


Figure 6. Regional RMSE between GTSM with the fine grid in two approaches and FES2014 for the whole of the year 2014 (cm). GTSM, Global Tide and Surge Model; RMSE, root mean square error.

ly for every month with both approaches. Contrary to the calibration period, where Approach 2 performed slightly better for the fine model, here Approach 1 generally shows marginally better results, except for the Indian Ocean.

In Figure 6, the RMSE between the model output and the observed value varies from month to month and also within the month. For example, the initial global average of RMSE in the calibration period is 5.23 cm, while it is 5.84 cm in the forecast period January 15–31, 2014, as Table 3 shows. One can observe that accuracy in the period January 15–31, 2014 is lower (higher RMSE) than the calibration period, both before and after calibration and independent of the approach. It fits our existing experience that the interaction between the various tidal constituent changes over time. However, the general conclusion is that the accuracy after the estimation has been greatly improved also for other forecast periods.

As examples, Figure 7 shows the spatial distribution of RMSE difference for GTSM with the fine grid in January 15–31 (a) and July (b) in Approach 1. Approach 2 shows a similar distribution to Approach 1 (not shown here). The spatial distribution of the RMSE difference in Figure 7 is similar to that in the calibration period. Most of the regions are improved but output in some regions is marginally worse than that in the

Table 3
Regional Forecast RMSE After Bathymetry Estimation in GTSM With Fine Grid in (cm) for Two Periods

RMSE	January 1–14			January 15–31		
	Initial	Approach 1	Approach 2	Initial	Approach 1	Approach 2
Arctic Ocean	5.24	3.98	4.34	5.93	4.27	4.92
India Ocean	5.57	4.21	3.62	6.04	4.12	4.01
North Atlantic	5.41	3.47	3.43	6.17	4.08	4.78
South Atlantic	5.69	4.40	3.96	6.14	4.45	4.67
North Pacific	4.15	3.32	3.11	5.42	4.40	4.58
South Pacific	5.57	3.73	3.43	6.30	4.17	4.48
Southern Ocean	4.28	3.04	2.97	4.51	2.97	3.34
Total	5.23	3.78	3.49	5.84	4.05	4.33

GTSM, Global Tide and Surge Model; RMSE, root mean square error.

initial model, which is even more obvious in the period January 15–31. The similar RMSE distribution in July demonstrates the excellent performance of the calibrated model for the long-term forecast.

In addition, we also evaluate the model performance in the frequency domain. Tidal analysis is based on the model output for the year 2014. The root-mean-square (RMS) between the model and the FES2014 data set in 1973 locations for major tide constituents are summarized in Table 4. For comparison with Stammer et al. (2014), we use the same formula for the RMSE per tidal component:

$$RMS = \sqrt{\overline{[A_m \cos(\omega t - \phi_m) - A_o \cos(\omega t - \phi_o)]^2}} \quad (15)$$

where A_m , A_o are the amplitudes from model output and observations. ϕ_m and ϕ_o are terms of phases lag. ω is the tide frequency. The overbar represents the computation over one full cycle of the constituent (e.g., ωt varying from 0 to 2π), as well as all the locations. A striking feature of the table is the lower RMS for the main components and the Root-Squared-Sum (RSS) over these components after the estimation in both author approaches. The M_2 component shows the largest change; it is reduced from 4.50 cm in the initial model to 2.25 and 2.54 cm for Approaches 1 and 2, respectively. The significant improvements of tide components for the estimated models demonstrate that they can be used for the long-term forecast.

A tidal analysis is also performed for the observation from Deep-Ocean Bottom Pressure Recorder (BPR) to compare GTSM with the model described by Stammer et al. (2014). We used model output for the full year of 2014 for this comparison. BPR data is available from the Supplement of Ray (2013). As an example, Table 5 shows the results from the NSWC (Naval Surface Weapons Center) model, FES2012, initial GTSM before calibration and estimated GTSM with Approach 2. The data of NSWC and FES2012 are from Table 3 in Stammer et al. (2014). In comparison to the seven purely hydrodynamic models in Stammer et al. (2014) (their Table 12), GTSM has an RMS for M_2 of 5.17 cm which is lower than other models except for the NSWC, which has an RMS of 4.27 cm for M_2 .

GTSM is further improved by the calibration but does not become as accurate as the modern assimilative tide models described by Stammer et al. (2014). For instance, the RMS of M_2 component and RSS for eight major components of the FES2012 model against deep ocean data in Table 5 are 0.66 and 1.12 cm, respectively, while GTSM with estimated bathymetry in Approach 2 are 2.55 and 3.96 cm for the RMS of M_2 and RSS, respectively. This is one of the reasons why we chose FES2014 data set to be used as observations for our deep ocean calibration. The main advantage of our calibration approach for GTSM is that it can also be straightforwardly applied for the studies of the effects of sea level rise, since surge can be included in the simulation by adding winds and air pressure to the forcing. For example, the first global reanalysis of storm surges and extreme sea levels (the GTSR data set) is presented based on the GTSM (Muis et al., 2016). In

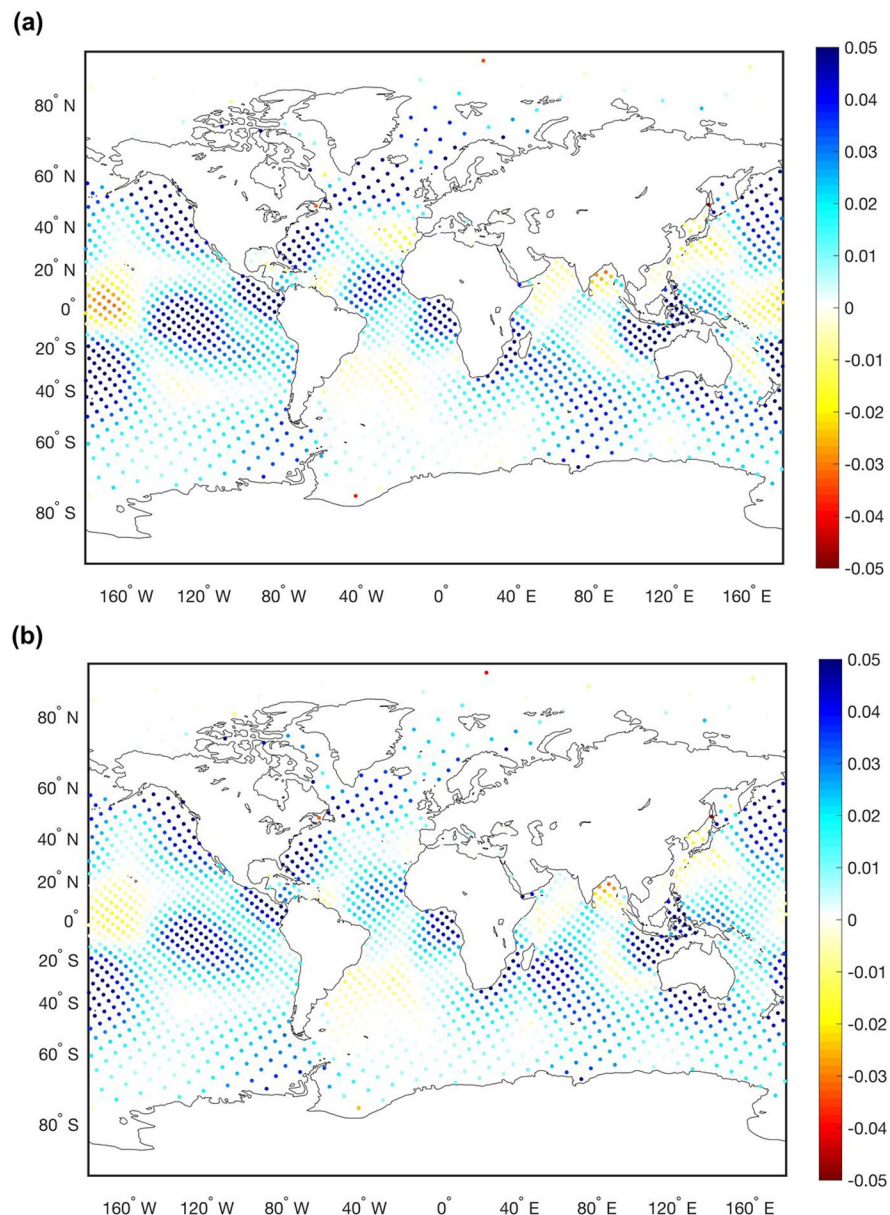


Figure 7. Spatial distribution of RMSE difference for GTSM with the fine grid in Approach 1 in the forecast period (a) January 15–31, 2014; and (b) July 1–31, 2014. The color blue shows improvement (unit: m). GTSM, Global Tide and Surge Model; RMSE, root mean square error.

Table 4
RSS and RMS of eight Major Tide Components Against FES2014 Data Set
in (cm)

Components	RMS for all locations								
	Q1	O1	P1	K1	N2	M2	S2	K2	RSS
Initial model	0.48	1.12	0.55	1.62	1.01	4.50	2.79	1.76	6.05
Approach 1	0.43	0.89	0.40	1.19	0.69	2.25	1.77	1.18	3.55
Approach 2	0.44	0.96	0.41	1.18	0.66	2.54	1.91	1.46	3.92

Section 5.2, we also applied the one-year sea level forecast to analyze the surge representation.

The amplitude and phase difference of M_2 component between GTSM with the fine grid and FES2014 data set is illustrated in Figure 8. Compared to the FES2014 data set, the differences in amplitudes and phases are substantially smaller in the estimated model for both approaches than the initial model. Approach 2 has a slightly better performance in amplitude (Figure 8c) than Approach 1 (Figure 8b), which is opposite in phases (Figure 8e and 8f).

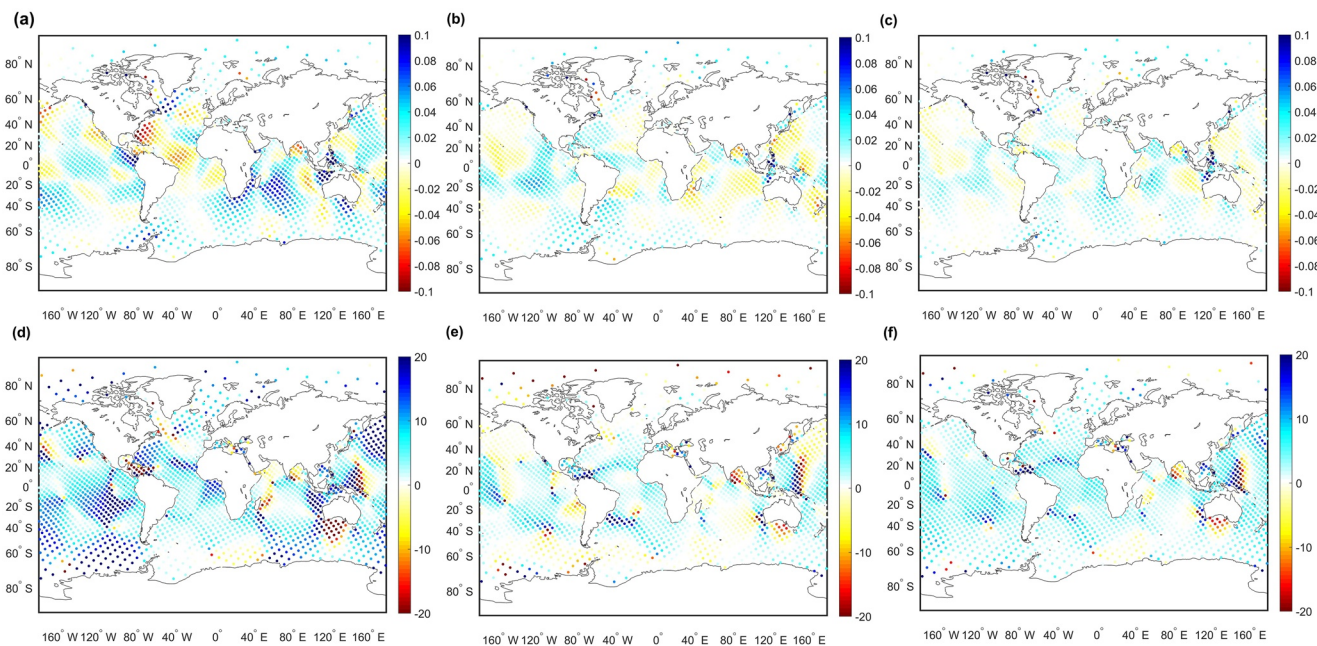


Figure 8. Spatial distribution of amplitude and phase difference of M_2 between the model and FES2014 data set. (a), (b), and (c): Amplitude difference for the initial GTSM, model estimated by Approach 1 and Approach 2, respectively (unit: m); (d), (e) and (f): Phases difference for the initial GTSM, model estimated by Approach 1 and Approach 2, respectively (unit: degree). GTSM, Global Tide and Surge Model.

5.2. Validation With UHSLC Tide Gauge Data

The calibrated models were also compared to UHSLC tide gauge data. Contrary to the selected FES data of the previous section, most of these locations are along the coast, and have one average large tidal amplitude with more pronounced local influences. The time periods used are the same set as above.

Figure 9 shows the spatial distribution of RMSE without estimation (Figure 9a) and RMSE difference for the tide output and data from 230 tide gauges for the calibration period from January 1 to 14, 2014 in Approach 2 (Figure 9b). Approach 1 (not shown here) reports a similar distribution to Approach 2. Most of the tide gauges are distributed in the coastal region. The RMSE in these locations (Figure 9a) is much larger than it in the deep ocean with the comparison of the FES2014 data set, which is as expected since tide constituents often have larger amplitudes in the coastal regions than in the deep ocean. The RMSE difference in Approach 1 is similar to that in Approach 2 and the RMSE difference in the coarse model is similar to it in the fine model. The model output from the estimated model is in better agreement with the UHSLC observations than the output from the initial model in the majority of the locations.

Table 5
RSS and RMS of eight Major Tide Components Against BPR Data Set in (cm)

Components	RMS for all locations								
	Q1	O1	P1	K1	N2	M2	S2	K2	RSS
NSWC ^a	0.29	0.87	0.64	1.29	1.15	4.27	1.78	0.66	5.11
FES2012 ^a	0.22	0.31	0.36	0.47	0.34	0.66	0.41	0.22	1.12
Initial Model	0.56	1.24	0.65	2.10	0.99	5.17	2.36	1.60	6.56
Approach 2	0.48	0.91	0.43	1.49	0.59	2.55	1.82	1.41	3.95

BPR, Bottom Pressure Recorder.

^aData of NSWC and FES2012 are from Table 3 in Stammer et al. (2014).

GTSM with the fine grid is more accurate than with the coarse grid, both before and after calibration. For example, RMSE in the initial GTSM before calibration with the coarse and fine grids are 17.23 and 12.98 cm, respectively. These are reduced to 13.49 cm in coarse grid and 11.12 cm in the fine grid after the estimation by Approach 1. Approach 2 shows similar results. In a relative sense the improvements in the calibration are quite significant, but less than in deep water. It is possible that resolution and more local influences play a larger role compared to deep water. This can also be seen when one compares the calibrated coarse model results to the initial fine model, where the calibration apparently can't compensate for the lower resolution. Still, both the coarse model and the fine model also benefit at the coast from a calibration that was performed using only data on deep water.

The performance of estimated models with the fine grid is analyzed further with a one-year prediction of tide and surge for the full year of 2014. Figure 10a shows the RMSE of the tide has improved significantly for both approaches and all months. Approach 1 performed slightly better than Approach 2. The spatial patterns of the tide RMSE in every month are very similar to the ones shown in Figure 9 and therefore not shown. Additional experiments with wind forcing (Figure 10b and 10c) show that the surge is much less sensitive to small adjustments of the bathymetry at large scales. The total water level, being the sum of tides and surge, benefits from the improved tides.

As an example, time series of the tide at station Benoa with the coordinate ($-8.75, 115.21$) from initial simulation and estimated simulation in January and July 2014 are shown in Figure 11a and 11b. The RMSE is decreased by $\sim 50\%$ in January and 59% in July for Approach 1, which is marginally better than for Approach 2 ($\sim 44\%$ and 52% , respectively).

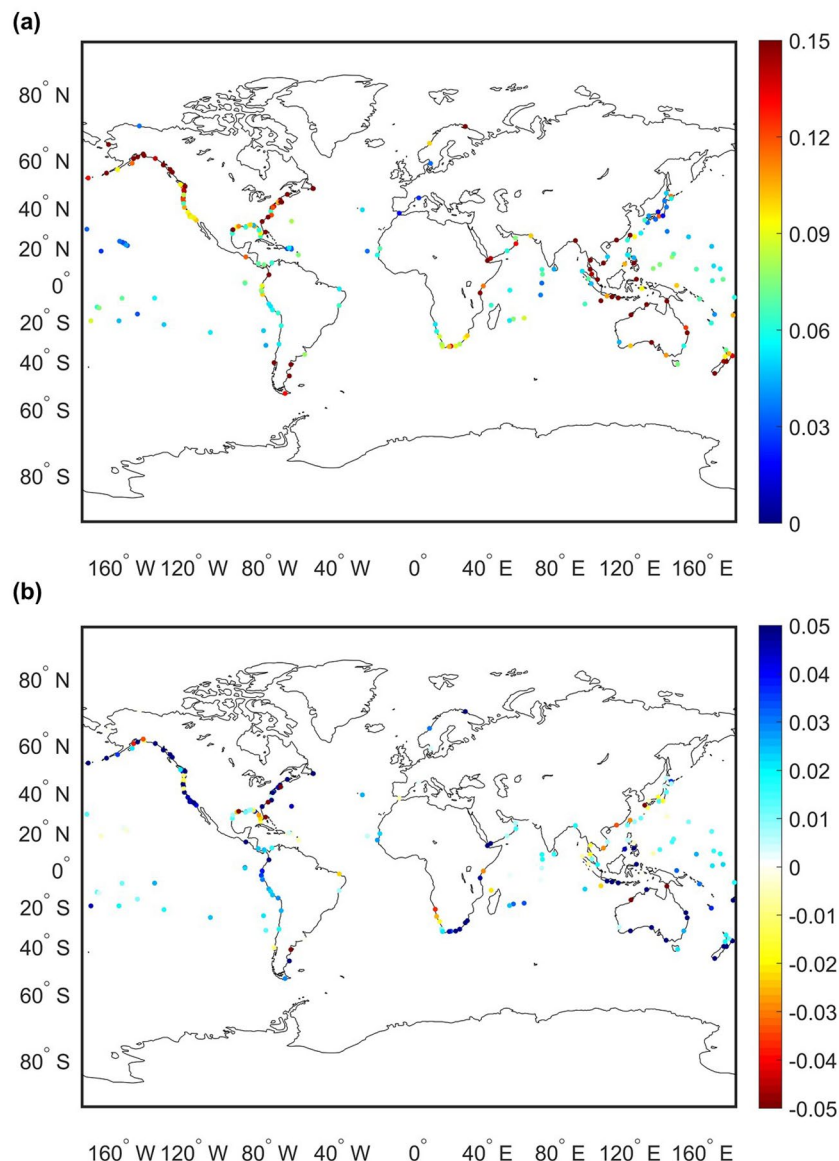


Figure 9. Spatial distribution of RMSE with the UHSLC data from January 1 to 14, 2014: (a) initial RMSE in fine GTSM; (b) RMSE difference in fine GTSM by Approach 2. RMSE differences shown in blue indicate improvement(unit:m). GTSM, Global Tide and Surge Model; RMSE, root mean square error.

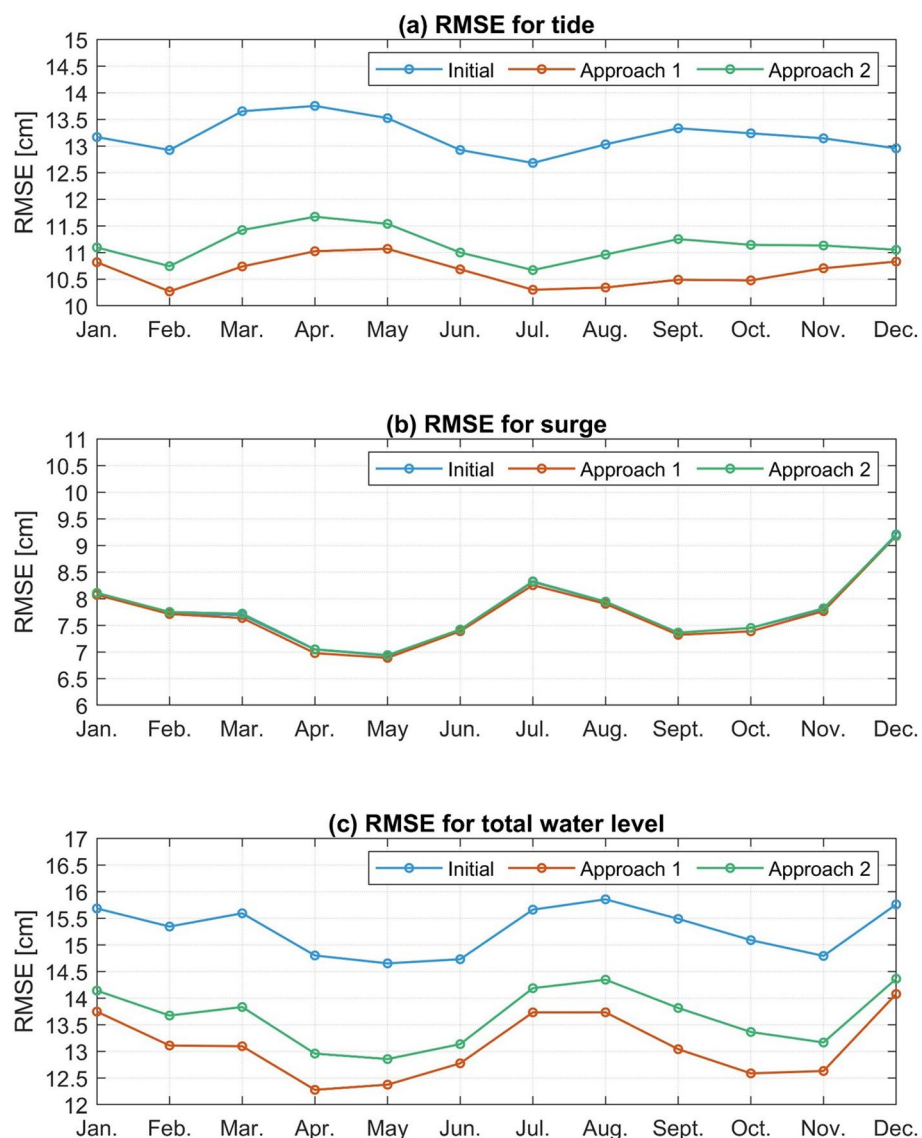


Figure 10. RMSE between GTSM with the fine grid in two approaches and FES2014 for the whole or the year 2014 (cm): (a) RMSE for tide; (b) RMSE for surge; (c) RMSE for total waterlevel. GTSM, Global Tide and Surge Model; RMSE, root mean square error.

Similar to the comparison to FES data, also for UHSLC tide gauges, Approach 2 performs best for the calibration period. Also here, the RMSE is higher for other periods than for the calibration period. This confirms our perception that the fine model generally improves most using Approach 2 during the calibration period, not just for the locations and data set used for the calibration. In other periods, the tidal constituents interact differently, leading to estimates that over-fit the data to some extent.

This problem can be solved by using a longer simulation time, such as one month, or even longer. However, longer simulation time means higher computational cost and larger storage requirement, which is out of reach for the current computing environment and implementation. Future work will attempt to solve this problem by modifying the algorithm.

We also note that the calibration changes the model performance significantly. However, in the current implementation the difference between the model output between the fine and the coarse models is only computed at the start. This can potentially be improved further. The algorithm in Approach 2 is similar to the inner loop of Incremental 4D-Var (Trémolié, 2007). The cost function in Incremental 4D-var is minimized

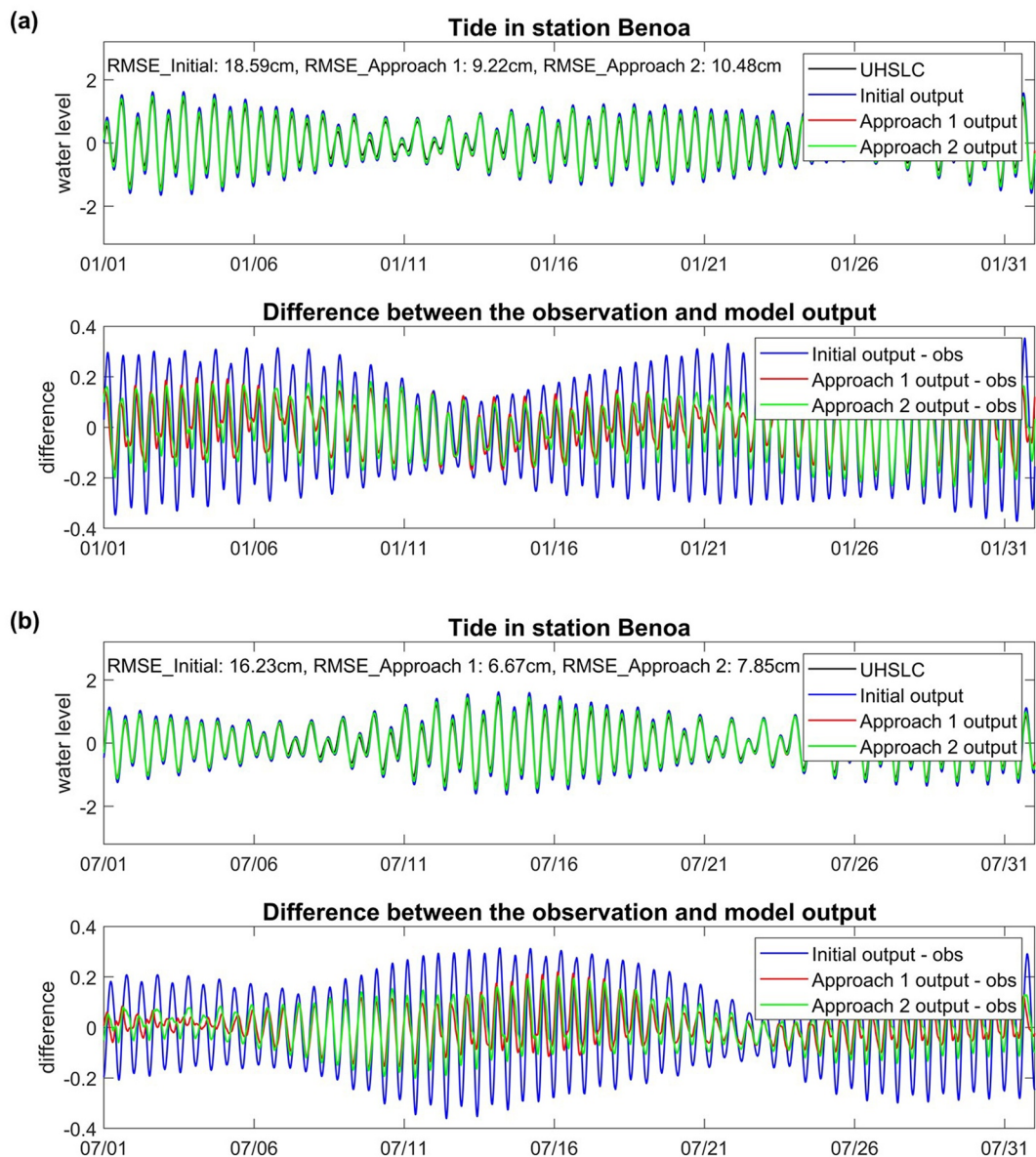


Figure 11. Tide elevation and difference comparison at station Benoa during (a) January and (b) July, 2014 (unit:m).

at a low resolution using an iterative algorithm (inner loop) and the resulting increment is then interpolated back to the high resolution and added to the current first guess (outer loop). A similar outer loop can also be implemented for Approach 2 in the future. The estimated parameters can be used as the new first guess to the inner loop. Because of the large computational cost, we have not performed this experiment yet, but we aim to do so in the future, after the algorithm has been optimized further.

6. Conclusions and Further Work

We have presented a complete application of parameter estimation for the high-resolution global tide and surge model (GTSM), with measurements from the FES2014 data set. A coarse-to-fine strategy is proposed by using output from the coarse model to replace the fine model during (parts of) the estimation, which effectively reduces the computational demand. Two variants of this approach were tested. Moreover, the computational demand and memory requirements are further reduced by maintaining only the most sensitive parameter dimensions, which were found through sensitivity experiments.

This study focuses on the estimation of bathymetry, which is considered to be the most influential parameter. A major challenge for estimation of bathymetry in a global tide model is the large computational cost. The optimization algorithm performs a large number of model simulations and even a single model in high resolution has an enormous computational cost, even when parallel computing is deployed. In this case, the coarse-to-fine strategy is applied to reduce the single model simulation time and make it computationally affordable for parameter estimation. We tested two approaches here: Coarse Calibration (Approach 1), where all model runs in the calibration are performed with a coarser model, and Coarse Incremental Calibration (Approach 2), where the model differences between initial model output and adjusted model output are replaced by a coarser model, but the observation model differences are computed with the fine model. Coarse Incremental Calibration requires one more fine model simulation than Coarse Calibration for the first guess. In our experiments the computational cost is reduced by a factor of approximately three based on these two approaches.

In addition to reducing the computing time in a single model, the number of model simulations also needs to be reduced, which is done here by reducing the number of parameters, because the initial number of simulations is proportional to the parameter dimension. To reduce the parameter dimension, a sensitivity test is performed by perturbing the bathymetry in a large number of spatial domains. First, the number of domains is reduced to 285 domains using an analysis based on the tide propagation length. Next a uniform correction factor is applied to the bathymetry for one domain at a time. Finally, using the computed sensitivity, we are able to decrease the number of parameters further to 110 domains. This number of 110 parameters is just feasible on the available computer infrastructure, with the existing implementation.

The optimization procedure leads to a significant reduction of the cost function for both approaches and to an improved fit to the FES2014 data for both the coarse and the fine versions of the model. Analysis from the frequency domain illustrates significant improvements, especially for the M_2 component, after the estimation. The estimation results are evaluated further by comparing model simulations for the whole of the year 2014 against the FES2014 data set and the UHSLC data set, which shows that although the calibration is performed for 2 weeks, this still results in a more accurate model for other time periods. Comparison to the mostly coastal tide gauges shows that the influence of resolution is more important there. The accuracy of the coarse model improves through calibration, but cannot exceed the accuracy of even the uncalibrated high-resolution model. On the other hand, the fine model benefits from the calibration even at coastal stations. The surge simulation further demonstrated that the estimated bathymetry is reasonable for not only tide prediction but also the long-term total water level prediction.

Experiments show that the parameter estimation scheme efficiently improves the accuracy of the GTSM modeled tides. Further work will concentrate on: The calibration algorithms work quite efficiently in terms of computation, but the experiments are now limited by the memory requirement for the inversion step in the DUD algorithm. At the same time, the results indicate that a longer time span for the calibration could be beneficial. A modification of the algorithm or parallelization of this step is necessary to test this. The increments in Approach 2 are now based on the initial fine model simulation. Somewhat similar to the outer loop in the incremental 4D-VAR, one can restart the algorithm with the updated fine model, which can potentially further improve the accuracy of the model. Finally, we have focused on calibration of the bathymetry throughout this study. Closer to the coast, the uncertainty related to bottom friction is probably important. The model performance may be further improved by the calibration of the more local bathymetry together with bottom friction, as well as using additional local observations. This will also provide an opportunity to verify if the friction can indeed be ignored for the initial calibration at the larger scales.

Data Availability Statement

Research Quality Data of UHSLC are available in University of Hawaii Sea Level Centre with the link <ftp://ftp.soest.hawaii.edu/uhslc/rqds>. GEBCO bathymetry datasets are provided by General Bathymetric Chart of the Oceans (https://www.gebco.net/data_and_products). BPR data are available from the Supplement of Ray (2013). FES2014 data set is acquired from <https://www.aviso.altimetry.fr>.

Acknowledgments

The first author wishes to thank the China Scholarship Council for providing financial support in terms of a scholarship grant. This work was carried out on the Dutch national e-infrastructure with the support of SURF Cooperative.

References

- Altaf, M. U., Verlaan, M., & Heemink, A. W. (2012). Efficient identification of uncertain parameters in a large-scale tidal model of the European continental shelf by proper orthogonal decomposition. *International Journal for Numerical Methods in Fluids*, 68(4), 422–450. <https://doi.org/10.1002/fld.2511>
- Arbic, B. K., Wallcraft, A. J., & Metzger, E. J. (2010). Concurrent simulation of the eddying general circulation and tides in a global ocean model. *Ocean Modelling*, 32(3), 175–187. <https://doi.org/10.1016/j.ocemod.2010.01.007>
- Barth, A., Alvera-Azcárate, A., Gurgel, K.-W., Staneva, J., Port, A., Beckers, J.-M., & Stanev, E. V. (2010). Ensemble perturbation smoother for optimizing tidal boundary conditions by assimilation of high-frequency radar surface currents application to the German bight. *Ocean Science*, 6(1), 161–178. <https://doi.org/10.5194/os061612010>
- Caldwell, P. C., Merrifield, M. A., & Thompson, P. R. (2015). *Sea level measured by tide gauges from global oceans—The joint archive for sea level holdings (NCEI accession 0019568)*, version 5.5. NOAA National Centers for Environmental Information. <https://doi.org/10.7289/V5V40S7W>
- Carre, L., & Lyard, F. (2003). Modeling the barotropic response of the global ocean to atmospheric wind and pressure forcing—comparisons with observations. *Geophysical Research Letters*, 30(6). <https://doi.org/10.1029/2002GL016473>
- Carre, L., Lyard, F., Cancet, M., Guillot, A., & Roblou, L. (2013). FES 2012: A new global tidal model taking advantage of nearly 20 years of altimetry. In L., Ouwehand (Ed.), *20 years of progress in radar altimetry*, ESA Special Publication (Vol. 710, Edn. 13, p. 13). Retrieved from <https://ui.adsabs.harvard.edu/abs/2013ESASP.710E..13C>
- Charnock, H. (1955). Wind-stress on a water surface. *Quarterly Journal of the Royal Meteorological Society*, 81(350), 639–640. <https://doi.org/10.1002/qj.49708135027>
- Cheng, Y., & Andersen, O. B. (2011). Multimission empirical ocean tide modeling for shallow waters and polar seas. *Journal of Geophysical Research*, 116(C11). <https://doi.org/10.1029/2011JC007172>
- Courtier, P., Thpaut, J.-N., & Hollingsworth, A. (1994). A strategy for operational implementation of 4d-Var, using an incremental approach. *Quarterly Journal of the Royal Meteorological Society*, 120(519), 1367–1387. <https://doi.org/10.1002/qj.49712051912>
- Dahle, C., Murbek, M., Flechtnner, F., Dobslaw, H., Michalak, G., Neumayer, K., et al. (2019). The GFZ GRACE RL06 monthly gravity field time series: Processing details and quality assessment. *Remote Sensing*, 11(18), 2116. <https://doi.org/10.3390/rs11182116>
- Das, S. K., & Lardner, R. W. (1991). On the estimation of parameters of hydraulic models by assimilation of periodic tidal data. *Journal of Geophysical Research*, 96, 15. <https://doi.org/10.1029/91JC01318>
- Edwards, C. A., Moore, A. M., Hoteit, I., & Cornuelle, B. D. (2015). Regional ocean data assimilation. *Annual Review of Marine Science*, 7(1), 21–42. <https://doi.org/10.1146/annurev-marine-010814-015821>
- Egbert, G. D., & Erofeeva, S. Y. (2002). Efficient inverse modeling of barotropic ocean tides. *Journal of Atmospheric and Oceanic Technology*, 19(2), 183–204. [https://doi.org/10.1175/1520-0426\(2002\)019<183:EIMBO>2.0.CO;2](https://doi.org/10.1175/1520-0426(2002)019<183:EIMBO>2.0.CO;2)
- Egbert, G. D., & Ray, R. D. (2000). Significant dissipation of tidal energy in the deep ocean inferred from satellite altimeter data. *Nature*, 405(6788), 775–778. <http://dx.doi.org/10.1038/35015531>
- Fok, H. S. (2012). *Ocean tides modeling using satellite altimetry*. Geodetic Science Rep. No. 501.
- González, A. (2009). Measurement of areas on a sphere using fibonacci and latitudelongitude lattices. *Mathematical Geosciences*, 42, 49–64.
- Hallegatte, S., Green, C., Nicholls, R., & Corfee-Morlot, J. (2013). Future flood losses in major coastal cities. *Nature Climate Change*, 3, 802–806. <https://doi.org/10.1038/nclimate1979>
- Heemink, A., Mouthaan, E., Roest, M., Vollebregt, E., Robaczewska, K., & Verlaan, M. (2002). Inverse 3D shallow water flow modeling of the continental shelf. *Continental Shelf Research*, 22(3), 465–484. [https://doi.org/10.1016/S0278-4343\(01\)00071-1](https://doi.org/10.1016/S0278-4343(01)00071-1)
- Irazoqui Apecechea, M., Verlaan, M., Zijl, F., Le Coz, C., & Kernkamp, H. (2017). Effects of self-attraction and loading at a regional scale: A test case for the northwest european shelf. *Ocean Dynamics*, 67(6), 729–749. <https://doi.org/10.1007/s10236-017-1053-4>
- Jongman, B., Ward, P. J., & Aerts, J. C. (2012). Global exposure to river and coastal flooding: Long term trends and changes. *Global Environmental Change*, 22(4), 823–835. <https://doi.org/10.1016/j.gloenvcha.2012.07.004>
- Kernkamp, H., Van Dam, A., Stelling, G., & de Goede, E. (2011). Efficient scheme for the shallow water equations on unstructured grids with application to the continental shelf. *Ocean Dynamics*, 1–14. <https://dx.doi.org/10.1007/s10236-011-0423-6>
- Kodaira, T., Thompson, K. R., & Bernier, N. B. (2016). The effect of density stratification on the prediction of global storm surges. *Ocean Dynamics*, 66, 1733–1743.
- Kuhlmann, J., Dobslaw, H., & Thomas, M. (2011). Improved modeling of sea level patterns by incorporating self-attraction and loading. *Journal of Geophysical Research*, 116(C11). <https://doi.org/10.1029/2011JC007399>
- Maraldi, C., Lyard, F., Testut, L., & Coleman, R. (2011). Energetics of internal tides around the Kerguelen plateau from modeling and altimetry. *Journal of Geophysical Research*, 116(C6). <https://doi.org/10.1029/2010JC006515>
- Mayo, T., Butler, T., Dawson, C. N., & Hoteit, I. (2014). Data assimilation within the advanced circulation (ADCIRC) modeling framework for the estimation of manning's friction coefficient. *Ocean Modelling*, 76, 43–58.
- Muis, S., Verlaan, M., Nicholls, R. J., Brown, S., Hinkel, J., Lincke, D., et al. (2017). A comparison of two global datasets of extreme sea levels and resulting flood exposure. *Earth's Future*, 5(4), 379–392. <https://doi.org/10.1002/2016EF000430>
- Muis, S., Verlaan, M., Winsemius, H., Aerts, J., & Ward, P. (2016). A global reanalysis of storm surges and extreme sea levels. *Nature Communications*, 7, 1–12. <https://doi.org/10.1038/ncomms11969>
- Openda User Documentation. (2016). Daltares.
- Pugh, D., & Woodworth, P. (2014). *Sea-level science: Understanding tides, surges, tsunamis and mean sea-level changes*. Cambridge University Press.
- Ralston, M. L., & Jennrich, R. I. (1978). Dud, A derivative-free algorithm for nonlinear least squares. *Technometrics*, 20(1), 7–14. <https://doi.org/10.1080/00401706.1978.10489610>
- Ray, R. D. (1999). *A global ocean tide model from topex/poseidon altimetry: GOT99. 2*. National Aeronautics and Space Administration Technical Memorandum. Goddard Space Flight Center.
- Ray, R. D. (2013). Precise comparisons of bottom-pressure and altimetric ocean tides. *Journal of Geophysical Research: Oceans*, 118(9), 4570–4584. <https://doi.org/10.1002/jgrc.20336>
- Savcenko, R., & Bosch, W. (2012). *EOT11A—empirical ocean tide model from multi-mission satellite altimetry*. Deutsches geodätisches forschungsinstitut (DGFI), Report No.89.
- Stammer, D., Ray, R. D., Andersen, O. B., Arbic, B. K., Bosch, W., Carrre, L., et al. (2014). Accuracy assessment of global barotropic ocean tide models. *Reviews of Geophysics*, 52(3), 243–282. <https://doi.org/10.1002/2014RG000450>

- Taguchi, E., Stammer, D., & Zahel, W. (2013). Inferring deep ocean tidal energy dissipation from the global high-resolution data-assimilative HAMTIDE model. *Journal of Geophysical Research: Oceans*, 119(7), 4573–4592. <https://doi.org/10.1002/2013JC009766>
- Ten Brummelhuis, P. G. J., Heemink, A. W., & van den Boogaard, H. F. P. (1993). Identification of shallow sea models. *International Journal for Numerical Methods in Fluids*, 17(8), 637–665. <https://doi.org/10.1002/fld.1650170802>
- Tozer, B., Sandwell, D. T., Smith, W. H. F., Olson, C., Beale, J. R., & Wessel, P. (2019). Global bathymetry and topography at 15 arc sec: SRTM15+. *Earth and Space Science*, 6(10), 1847–1864. <https://doi.org/10.1029/2019EA000658>
- Trémolet, Y. (2007). Incremental 4d-Var convergence study. *Tellus A*, 59(5), 706–718. <https://doi.org/10.1111/j.1600-0870.2007.00271.x>
- Verlaan, M., De Kleermaeker, S., & Buckman, L. (2015). *GLOSSIS: Global storm surge forecasting and information system (online)*. Paper presented at 22nd Australasian Coastal and Ocean Engineering Conference and the 15th Australasian Port and Harbour Conference, 229–234. Engineers Australia and IPENZ.
- Weatherall, P., Marks, K. M., Jakobsson, M., Schmitt, T., Tani, S., Arndt, J. E., et al. (2015). A new digital bathymetric model of the world's oceans. *Earth and Space Science*, 2(8), 331–345. <https://doi.org/10.1002/2015EA000107>
- Zaron, E. D. (2017). Topographic and frictional controls on tides in the sea of Okhotsk. *Ocean Modelling*, 117, 1–11. <https://doi.org/10.1016/j.ocemod.2017.06.011>
- Zaron, E. D. (2019). Simultaneous estimation of ocean tides and underwater topography in the Weddell sea. *Journal of Geophysical Research: Oceans*, 124(5), 3125–3148. <https://doi.org/10.1029/2019JC015037>
- Zijl, F., Verlaan, M., & Gerritsen, H. (2013). Improved water-level forecasting for the northwest European shelf and North Sea through direct modelling of tide, surge and non-linear interaction. *Ocean Dynamics*, 63(7), 823–847. <https://doi.org/10.1007/s10236-013-0624-2>